Placode and neural crest origins of congenital deafness in mouse models of Waardenburg-Shah syndrome

Jamie Vicente S. Tan[1], Alicia Duron[1], Henry M. Sucov[2], and Takako Makita[1]

[1] Darby Children's Research Institute, Department of Pediatrics, Medical University of South Carolina, Charleston, SC 29425, USA

[2] Department of Regenerative Medicine and Cell Biology, Medical University of South Carolina, Charleston, SC 29425, USA

Corresponding author: Takako Makita (makita@musc.edu)

Abstract

Mutations in the human genes encoding the endothelin ligand-receptor pair *EDN3* and *EDNRB* cause Waardenburg-Shah syndrome (WS4), which includes congenital hearing impairment. The current explanation for auditory dysfunction is a deficiency in migration of neural crest-derived melanocytes to the inner ear. Here, we have explored the role of endothelin signaling in auditory development in mice using neural crest-specific and placode-specific *Ednrb* mutation. We find a normal representation of neural crest lineage labeled melanocytes in hearing impaired mutant mice. Instead, our results implicate a previously unrecognized role for glial support of synapse assembly between auditory neurons and cochlear hair cells. In addition, placode-specific *Ednrb* mutation also caused impaired hearing resulting from deficient synaptic transmission. Our observations challenge the current understanding of endothelin signaling in auditory development, invoke independent and separable roles in the neural crest and placodal lineages, and expand the scope of processes that utilize endothelin signaling to create a functional auditory circuitry.

Introduction

The auditory system arises from two distinct ectodermal lineages, placode and neural crest. The placode-derived otic vesicle gives rise to the cochlea including mechanosensory hair cells, supporting cells, and the non-melanocyte populations of the stria vascularis. Epibranchial placodes exclusively give rise to spiral ganglion (auditory) neurons (SGNs); these are bipolar neurons that extend peripheral axons to the hair cells and also project into an ascending auditory pathway (the dorsal and ventral cochlear nuclei) of the central nervous system (Barald and Kelley 2004; Ladher et al. 2010). SGNs are specified into two functionally distinct types: type I neurons establish afferent synapses on inner hair cells (IHCs), and type II neurons extend afferent axon branches and synapse on outer hair cells (OHCs). The hair cells reside in the cochlear duct, a compartment filled with potassium-enriched endolymph which provides the electrochemical environment that is crucial for hair cell mechanotransduction. The ionic composition (endocochlear potential) of endolymph is maintained by neural crest-derived melanocytes that comprise the intermediate cell layer of the stria vascularis (Steel and Barkway 1989). Neural crest also gives rise to glia, including satellite cells that enfold individual SGNs in the spiral ganglia, and Schwann cells that are associated with peripheral auditory nerve fibers (D'Amico-Martel and Noden 1983). In mammals, the final establishment of normal auditory circuitry occurs postnatally (in mice, over the first 2 postnatal weeks). Developmental perturbations that result in defective hair cell mechanotransduction and/or defective mechanosensory circuitry result in congenital sensorineural hearing impairment or deafness, which is a significant human burden (Pingault et al. 2010; Johnson et al. 2019). While the anatomical composition of the normal auditory system is well defined, many of the molecular features that underlie the developmental and maturation events that create auditory functionality or that result in dysfunction are not well studied.

Waardenburg syndrome (WS) is a human congenital disorder characterized by pigmentation abnormalities and sensorineural deafness, and is classified into 4 subtypes based on additional phenotypic components (Gettelfinger and Dahl 2018). Type 4 Waardenburg syndrome (WS4), also called Waardenburg-Shah syndrome, is distinguished from other WS types because of its association with a congenital gut motility disorder known as Hirschsprung disease (HSCR) (Read and Newton 1997). Mutations in genes encoding endothelin receptor type B (EDNRB) and its ligand endothelin 3 (EDN3) are prominently associated with human WS4 (Huang et al. 2022). Importantly, EDN3-EDNRB pathway gene mutations are also found in HSCR patients without WS pathologies, indicating variable penetrance of auditory and pigmentation phenotypes.

HSCR and WS4 are examples of a large class of congenital syndromes called neurocristopathies that involve neural crest cells as a common etiologic factor (Mueller and Goldstein 2022). Defective migration of neural crest cells to a variety of sites including skin, hair, inner ear, and gastrointestinal tract is believed to account for all pathological features demonstrated in human WS4. Thus, HSCR is characterized by a failure of enteric nervous system progenitors to migrate into the distal colon, which results in an aganglionic segment in the terminal bowel and thereby a failure of colonic peristaltic contraction. Similarly, melanocytes (pigment cells) throughout the body arise from the neural crest and their deficiency explains pigmentation abnormalities in human WS. In mouse, Edn3-Ednrb gene mutations recapitulate human WS and HSCR disease pathologies including aganglionic colon and coat color pigmentation defects (Baynash et al. 1994; Hosoda et al. 1994). Mouse mutants were also reported to not have neural crest-derived intermediate melanocytes in the stria vascularis of the inner

ear, which like HSCR and coat color alterations could result from a melanocyte migration defect (Matsushima et al. 2002). These melanocytes generate the endocochlear potential and are essential for hearing, so their absence would explain deafness. To date, absence of neural crest-derived melanocytes in the stria vascularis is accepted as the primary etiology of sensorineural deafness in WS4.

In this study, we utilized the genetically diverse outbred ICR mouse strain background to examine auditory function in Edn3-Ednrb global and conditional mutant mice. Unlike prior mouse studies but as observed in humans, all mutant mice exhibited aganglionic colon (HSCR) whereas hearing impairment was variably penetrant. We make two additional key observations. First, hearing impaired mutant mice on this strain background have a normal contribution of melanocytes to the stria vascularis. This challenges the conclusion that deafness in WS is the result of stria melanocyte migration deficiency; our results instead point to a glial-specific (neural crest) role in mechanosensory synapse formation. Second, we show that there is an independent required role for Edn3-Ednrb signaling within the placode lineage to enable auditory functionality. Here, our results implicate an SGN-specific role in synaptic transmission. Our findings establish a dual lineage origin of congenital hearing loss in Edn3-Ednrb type WS4, force reevaluation of the paradigm for auditory defects in the context of these mutations, and demonstrate the complex genetics that cause Ednrb deficiency to manifest in auditory function above or below a hearing threshold.

Results

Incomplete penetrance of hearing loss in endothelin signaling mutant mice

Genetic background affects the penetrance and expression of many phenotypes. Variable degrees of

pigmentation abnormalities and colonic aganglionosis in *Ednrb* null rodents are examples of this dynamic (Dang et al. 2011). Auditory defects, however, have either been present or absent in these rodent models with no indication of variable penetrance (Matsushima et al. 2002; Ida-Eto et al. 2011). We performed click-evoked auditory brain response (ABR) on *Ednrb*- and *Edn3*-null mutant mice that have been maintained in the genetically diverse outbred ICR background. All homozygous mutants for the global *Ednrb* or *Edn3* alleles died within a few days of postnatal day 21 with chronic constipation from colonic aganglionosis (i.e., HSCR). All animals including control littermates were therefore subjected for ABR at postnatal day 18-19, and their hearing (ABR threshold) determined as the lowest intensity at which a representable ABR waveform could be visually identified. All control mice (Supplemental Table S1) showed response in the range of 50-70 sound pressure level (dB SPL) (Fig 1a-b). In 41 global *Ednrb* mutant mice (from 15 litters generated from 8 independent breeding pairs), 17 mutants showed no response even at the highest sound pressure level (>90dB) and 12 mutants showed an ABR threshold at 80 or 90dB. Surprisingly, 12 mutants showed a comparable response to littermate controls (ABR threshold ≤70dB). These were bilateral traits; mutants with hearing impairment on one ear exhibited impaired hearing on the other ear and mutants that showed normal hearing on one ear also demonstrated normal hearing on the other ear. Overall, 71% of global *Ednrb* mutant mice exhibited hearing impairment (ABR threshold ≥80dB or no response). Similarly, 61% of global *Edn3* null mice (76 mice from 27 litters generated from 14 independent breeding pairs) showed hearing impairment (19 with no response, 27 with ABR threshold ≥80dB, 30 with ABR threshold ≤70dB). Thus, in this outbred background, auditory defects were very prominent but incompletely penetrant, whereas HSCR was fully penetrant. This resembles the presentation of defects in humans with *EDN3* or *EDNRB* gene mutations. Because ICR background mice are albino, pigmentation phenotypes could not

be scored.

Edn3-Ednrb signaling is essential not only in neural crest but also in placode lineage for hearing

Although the biological role of Edn3-Ednrb signaling has been demonstrated in neural crest migration, Ednrb expression in the cochlea is not limited to only melanocytes of the stria vascularis. We defined the sites of Ednrb expression using *Ednrb-eGFP* BAC transgenic mice at P7, a time by which type I and type II SGN specification and their axon pruning to the inner and outer spiral bundles is already complete. Ednrb expression was detected by GFP immunofluorescence in the lateral wall of the cochlea (stria vascularis) as well as along the entire axis of the spiral ganglia (Fig 2a). In the spiral ganglia, Ednrb expression was associated with Tuj1$^+$ SGNs (Fig. 2b) and Tuj1$^+$ (including both afferent and efferent) nerve fibers innervating both IHCs and OHCs (Fig. 2c-2e), and with BLBP$^+$ satellite glia (Fig. 2d) and BLBP$^+$ and BLBP$^-$ Schwann cells (Fig. 2e). In the stria vascularis, Kir4.1 channel-expressing intermediate cells and Kir4.1$^-$ basal cells expressed Ednrb-EGFP but not Kir4.1$^-$ marginal cells (Fig. 2f). Many but not all epithelial cells of Reissner's membrane (Fig. 2f) and subsets of PECAM$^+$ vascular endothelial cells (Fig. 2g) also expressed Ednrb throughout the cochlea. We did not detect Ednrb expression in mechanosensory hair cells (IHCs and OHCs) or supporting cells (Fig. 2c) at this time point.

Because of this broad expression domain, we evaluated the tissue specific roles of *Ednrb* gene in auditory development. For this purpose, we used *Wnt1Cre* and *Pax2Cre* to drive conditional gene recombination in the neural crest and placode lineages, respectively. When combined with the conditional lineage tracer *R26$^{nT\text{-}nG}$*, *Wnt1Cre* activity (visualized by nuclear GFP) was limited to BLBP$^+$ satellite cells of the spiral ganglion (Fig 3a, 3b), BLBP$^+$ and BLBP$^-$ Schwann cells that are associated with

auditory nerve fibers (Fig. 3a, 3c), and Kir4.1^{+} intermediate cells (melanocytes) of the stria vascularis (Fig 3a, 3d). *Pax2Cre* is active within Hu^{+} SGNs (Fig. 3e, 3f) including Peripherin^{+} type II SGNs (Fig. 3g), and in a variety of cell types in the cochlear duct including hair cells, supporting cells, fibrocytes and epithelium (Fig. 3e). There was no obvious overlap in active domains of *Wnt1Cre* and *Pax2Cre*, although because both are Cre lines they cannot be combined to confirm this point. In spiral ganglia, *Pax2Cre* labeled 94.8±1.1% of SGNs (n=632 from 13 cochlea) and *Wnt1Cre* delineated 95.4±1.0% of satellite cells (n=498 from 11 cochlea). Based on the immunolabeling and morphological assessment, *Wnt1Cre* recombination efficiency in the intermediate stria cells was 93.4±1.1% (n=151 from 10 cochlea). We also documented high efficiency and specific recombination by *Tbx18Cre*, *Phox2bCre*, and *Tie2Cre* in otic fibroblasts (Supplemental Fig. S2a), auditory efferent nerves (Supplemental Fig. S2b), and vascular endothelial cells (Supplemental Fig. S2c), respectively.

We crossed each of these Cre drivers with a conditional *Ednrb* allele and performed a large scale ABR screen at P19. The analysis included 206 *Wnt1Cre/Ednrb* mutants (92 litters from 39 breeding pairs), 237 *Pax2Cre/Ednrb* mutants (103 litters from 36 breeding pairs), 12 *Tbx18Cre/Ednrb* mutants (4 litters from 4 breeding pairs), 15 *Phox2bCre/Ednrb* mutants (9 litters from 5 breeding pairs) and 16 *Tie2Cre/Ednrb* mutants (4 litters from 2 breeding pairs)(Fig. 1a). Controls included Cre-positive and *Ednrb* heterozygous mice from these same litters (Supplemental Table S1). Hearing impairment was evident in both *Wnt1Cre/Ednrb* and *Pax2Cre/Ednrb* with incomplete penetrance (57% and 59%, respectively), just as observed in global *Ednrb* and *Edn3* mutant mice. Thus, the neural crest and placode lineages are both independently critical for Ednrb-mediated auditory functionality. All *Tbx18Cre/Ednrb*, *Phox2bCre/Ednrb* and *Tie2Cre/Ednrb* mutants exhibited ABR thresholds comparable

to controls (Fig. 1a-1b).

To further define hearing impairment observed in these mice, we tested selected global *Ednrb* (n=8), global *Edn3* (n=14), *Wnt1Cre/Ednrb* (n=15) and *Pax2Cre/Ednrb* (n=13) mutants that were ABR non-responsive at 90dB for Distortion Product Otoacoustic Emissions (DPOAEs) at P20. All of these deaf mice presented a comparable DPOAE response to control mice (n=26) in the stimulus range of 4-32 kHz, indicating that cochlear amplifier function is fully intact in all four mutant backgrounds (Fig. 1c).

We further evaluated the ABR waveforms of hearing (ABR threshold ≤70dB) and hearing impaired (ABR threshold 80 or 90dB) mutants in each of these four mutant backgrounds. Wave I represents the activity of primary afferent neurons (SGNs), and its amplitude reflects the stimulus intensity and the number of mechanosensory axons that are simultaneously activated, whereas its latency reflects the duration between the initial stimulus and the peak of wave. Hearing impaired mutants of all four genotypes exhibited significantly lower wave I amplitude and longer latency compared to their controls at the stimulus intensity range (90dB and 80dB) at which they responded (Fig. 1d, Supplemental Fig. S1). This indicates activation of fewer SGNs and less synchronicity in SGN activation upon stimulation. Interestingly, although not as severely compromised as in hearing impaired mutants, hearing mutants (i.e., mutants with ABR threshold ≤70dB) also displayed less amplitude and longer latency relative to controls; this was statistically significant in *Wnt1Cre/Ednrb* and *Pax2Cre/Ednrb* mutants because of greater sample number but also showed the same trend in global mutants (Fig. 1d). The high specificity and recombination efficiency of *Pax2Cre* and *Wnt1Cre* imply that variable recombination does not explain phenotypic range and penetrance. Rather, we suggest that additional genetic factors

(phenotypic modifiers) in the diverse genetic background of our outbred colony converge with Edn3-Ednrb to determine whether hearing is normal, impaired, or fully absent (see Discussion).

Melanocyte deficiency is not associated with hearing impairment in *Ednrb*-deficient mice

The etiology of hearing loss in WS4 is thought to result from impaired migration of neural crest-derived melanocytes to the stria vascularis. To address the presence or absence of cochlear melanocytes in *Wnt1Cre/Ednrb* mutant mice, we crossed the $R26^{td\text{-}Tomato}$ reporter into the *Wnt1Cre/Ednrb* background and visualized neural crest-derived cells at P19 in the cochlea of 6 hearing mutants and 15 hearing impaired mutants generated from 3 independent breeding pairs (Fig. 4). Surprisingly, in both hearing (ABR threshold ≤70dB) and hearing impaired mutants, *Wnt1Cre*-labeled cells were present in the intermediate layer of the stria vascularis. Moreover, these cells were functionally mature as evidenced by expression of the inwardly rectifying potassium channel Kir4.1. In several mutants we observed various mild anomalies including a partial loss of *Wnt1Cre*-labeled cells (Fig. 4c, 4e, 4g), a partial loss of Kir4.1 expression in *Wnt1Cre*-labled intermediate stria cells (Fig. 4c. 4e, 4g), and misexpression of Kir4.1 in non-Wnt1Cre-labeled marginal cells (Fig.4c, 4g). However, these anomalies were also present in hearing mutants (Fig. 4g). Significantly, the majority of hearing impaired mutants (and of hearing mutants) had a fully normal organization of the stria vascularis. Although very few were analyzed in this manner, we also observed normal population and maturation of intermediate stria cells in global *Ednrb* deaf mutants (Fig. 4f, 4g). Thus, in the ICR background of this colony, cochlear melanocyte defects in *Ednrb* mutants are variably penetrant and at most are limited in scale. More importantly, melanocyte deficiency cannot be the primary cause of hearing loss.

Contribution of glial *Ednrb*-deficiency to defective mechanosensory synapse formation

If melanocyte deficiency in the stria vascularis does not explain hearing impairment, we asked if hearing loss instead arises from auditory nervous system defects. We performed immunofluorescence analysis for Tuj1, synaptophysin (SYP), and C-terminal-binding protein 2 (CtBP2) in *Wnt1Cre/Ednrb* mutant cochlea to evaluate auditory nerve fibers, auditory synapses, and synaptic ribbon profiles. In control cochlea at P19, Tuj1$^+$ nerve fibers have assembled synaptic connection at IHCs and OHCs, as shown by the juxtaposition of presynaptic CtBP2 and postsynaptic SYP (Fig. 5a). Whereas hearing mutants displayed almost normal pre- and postsynaptic assembly (Fig. 5b, 5f, 5g), in hearing impaired mutants there was notable disorganization of CtBP2$^+$ synaptic ribbons on both inner and outer hair cells (Fig. 5c, 5e, 5g). This was particularly prominent at OHCs (Fig. 5g), but also observed at IHCs (Fig. 5e). Synaptic ribbons facilitate rapid, precise and continuous neurotransmission and are critical for auditory perception. Postsynaptic SYP showed a corresponding pattern, being more altered in hearing impaired OHCs (Fig. 5f) than IHCs (Fig. 5d). As SYP staining represents both efferent and afferent synapses, the disruption of afferent SYP$^+$ synapses at both IHCs and OHCs in hearing impaired *Wnt1Cre/Ednrb* mutants is likely much greater than what is presented and quantified in Fig 5. These results imply that defective mechanosensory synapse formation is the primary phenotype that accounts for auditory impairment in *Wnt1Cre/Ednrb* mutants. Without proper afferent synaptic organization, auditory function would be compromised or eliminated.

Wnt1Cre is not active in SGNs nor in their primary afferent targets (IHCs and OHCs), all of which are placode-derived. *Wnt1Cre* is active in the mid/hindbrain region which includes the olivocohlear nuclei, from which efferent nerves originate. For two reasons this source is unlikely to contribute to auditory

impairment in *Wnt1Cre/Ednrb* mutants. First, the efferent system is primarily involved in auditory discrimination and cellular protective roles rather than in primary auditory perception and so is outside the realm of ABR measurement. More decisively, *Ednrb* conditional mutation with efferent nerve-specific *Phox2bCre* did not result in hearing impairment (Fig. 1a). The one remaining *Wnt1Cre* sublineage that could plausibly account for defective synapse formation is glia. *Wnt1Cre*-labeled glial cells are abundantly present in the cochlea, as satellite cells tightly associated with spiral ganglia neurons (Fig. 3b) and as Schwann cells associated with afferent nerve fibers (Fig. 3c). Satellite cells and Schwann cells both express Ednrb (Fig. 2). Glial cells play important roles in many aspects of neural development and maturation, including synapse formation in both central and peripheral nervous system (Hanani and Verkhratsky 2021). Anatomically, there was no obvious disruption in the number or distribution of glial cells in the spiral ganglia of mutant mice (Supplemental Fig. S3). This suggests a functional deficiency in glial cells as the underlying condition that results in hearing impairment. Because we observe a synaptic defect between SGNs and hair cells, both of which are placode-derived, these results imply an initial endothelin-dependent signaling process in glia that secondarily supports SGN synapse organization at hair cells, and which is compromised in hearing impaired *Wnt1Cre/Ednrb* mutants.

<u>An intrinsic requirement for Ednrb in type I SGN activation/excitation</u>

Unlike *Wnt1Cre/Ednrb* mutants, hearing impaired *Pax2Cre/Ednrb* mutant mice displayed normal presynaptic CtBP2 and postsynaptic SYP profiles at both IHCs and OHCs (Supplemental Fig. S4a-4c). This suggested that the underlying cell and molecular events that impact on auditory perception in *Pax2Cre/Ednrb* mutants are different from the synapse defect observed in *Wnt1Cre/Ednrb* mutant

mice. *Pax2Cre* is active in the majority of otic cell types (Fig. 3e), although Ednrb is not expressed in most of these that are relevant for auditory function (e.g., hair cells, supporting cells, etc.). *Pax2Cre* denotes subsets of Ednrb-expressing otic fibrocytes, but the normal hearing of *Tbx18Cre/Ednrb* mutants (Fig. 1) refutes basal stria cells (Supplemental Fig. S2b) as the cause of hearing impairment. SGNs are the main cell type that is within the *Pax2Cre* recombination domain and expresses Ednrb, suggesting an intrinsic requirement for Ednrb function in SGNs. Although postsynaptic SYP labeling at sensory hair cells was normal, we noted a significant reduction in vesicular SYP staining in *Pax2Cre/Ednrb* mutant SGNs (Fig. 6c). This phenotype was observed in all hearing impaired *Pax2Cre/Ednrb* mutants analyzed, whereas SGNs of hearing *Pax2Cre/Ednrb* mutants showed comparable levels of vesicular SYP^+ area to control mice (Fig. 6a-6c, 6g). Vesicular transport in neurons is a reflection of synaptic transmission. Thus, these observations suggest that *Ednrb* deficiency in SGNs results in impaired neural activation.

Glutamate is the primary neurotransmitter released by hair cells to activate SGNs, which receive this signal via AMPA receptors (Reijntjes and Pyott 2016). To test if impaired glutamate signaling accounts for reduced SGN activity in hearing impaired *Pax2Cre/Ednrb* mutant mice, we examined the expression and localization of the AMPAR subunit GluR2 and presynaptic CtBP2. We screened a total of 17 hearing impaired *Pax2Cre/Ednrb* mutants and 7 hearing *Pax2Cre/Ednrb* mutants. In hearing *Pax2Cre/Ednrb* mutants, $GluR2^+$ clusters were detected at IHCs at a comparable level to control IHCs (Fig. 6e, 6h), and each $GluR2^+$ clusters was located in conjunction with a presynaptic $CtBP2^+$ puncta (Fig. 6e, 6i), as also observed at IHCs of control mice (Fig. 6d, 6h-6i). However, in hearing impaired *Pax2Cre/Ednrb* mutant mice, the number of $GluR2^+$ clusters on average was significantly reduced, although those $GluR2^+$

clusters that were present at IHCs were properly juxtaposed with CtBP2 (Fig. 6f, 6h-6i). Interestingly, this GluR2 abnormality was found in 13 out of 17 hearing impaired *Pax2Cre/Ednrb* mutants (Fig. 6h-6i); the remaining 4 hearing impaired mutants (Fig. 6h-6i; arrows) exhibited a normal number of GluR2$^+$ clusters even as they still presented an impaired vesicular SYP$^+$ profile (Fig. 6c, 6g). This divergence is unlikely to simply be measurement error but more likely reflects phenotypic variation. In sum, in hearing impaired *Pax2Cre/Ednrb* mutants, alteration of vesicular SYP and reduced GluR2 localization together lead to the conclusion that the primary lesion is an SGN-autonomous defect in synaptic transmission. As also for *Wnt1Cre/Ednrb* mutants, the variable penetrance of hearing phenotypes is inferred to reflect the activity of unlinked genetic alleles (modifiers) that are variable between individual mice in this study.

Discussion

Congenital deafness is among the more prevalent chronic conditions seen in human infants. Genetic causes are thought to explain the majority of cases in developed countries. In many cases the genetic basis of deafness is unknown, and even where causative gene mutations are known, the explanation for how these are transduced into auditory development or function has often been unclear. In this analysis of *Edn3* and *Ednrb* mutant mice, we reach several new insights that have not been appreciated in prior studies: a deficiency of melanocyte migration to the stria vascularis does not explain deafness in this WS4 model, endothelin-dependent glial support of SGN synaptogenesis is a previously unrecognized feature of auditory development, and an endothelin-dependent autonomous process in SGN synaptic transmission is a separate and independent cause of deafness. To a significant extent, these insights were possible to recognize because of the outbred genetic background of our colony. In

addition, we could distinguish these processes through tissue-specific conditional analysis that has not previously been conducted.

The paradigm that melanocyte migration deficiency explains deafness in Waardenburg syndromes and in particular in WS4 is strongly entrenched. This is reasonable: Hirschsprung disease represents migration failure of enteric progenitors to the colon, pigmentation defects represent failure of melanocyte migration into the skin, and the intermediate cells of the stria vascularis are melanocytes that derive from neural crest and must migrate to become incorporated into the inner ear. It is worth noting that numerous other neural crest lineages that also require migration do so normally in *Edn3* and *Ednrb* mutants and in other WS models (e.g., dorsal root and sympathetic chain ganglia, the outflow tract of the heart, adrenal medulla, etc.), so impaired migration of stria intermediate cells in *Edn3* or *Ednrb* mutants is not a foregone conclusion. Nonetheless, several past studies (Matsushima et al. 2002; Ida-Eto et al. 2011) of *Ednrb* rodent models (*Edn3* has not been studied in this regard) have documented a melanocyte deficiency which we do not see in our mice. One possibility is that melanocyte migration is better supported in the strain background (ICR) of our mice. Regardless, our results indicate that endothelin signaling has multiple roles in the neural crest lineage of the inner ear, including in auditory synaptic assembly as observed here. This latter role has not been previously recognized.

We note that our assessment of mature melanocytes in the stria vascularis is based on the visible presence of neural crest lineage-labeled cells expressing Kir4.1, but this is not a functional assessment of endocochlear potential. Alternatively, our studies implicate glial cells as a candidate site of Ednrb

activity to explain deafness in *Wnt1Cre/Ednrb* mutants. To a certain extent, our interest in glia is based on exclusion of other candidate neural crest cell types (melanocytes and cranial efferent nerves). Formal proof of a glial-specific role will require an appropriate glia-specific Cre line which we do not yet have. Nonetheless, such a role is quite reasonable: it is known in other contexts that glia modulate several aspects of neuronal development and function. Furthermore, glial cells are a major subpopulation of neural crest and they express Ednrb. We propose that glial cells, in response to Edn3 and mediated through Ednrb, are induced to either secrete paracrine factors that promote SGN synaptic assembly or express products that promote SGN synaptic assembly through cell-cell contact.

Our studies have also revealed a placode-specific role for endothelin signaling. A hint of this role appeared in one prior study in which transgenic reexpression of Ednrb in SGNs of global *Ednrb* mutant mice resulted in partial improvement in hearing (Ida-Eto et al. 2011). This was associated with rescue of SGN neurodegeneration, which is a phenotype that we do not see in our global and conditional mutant mice. Instead, our data implicate SGN synaptic transmission as the primary lesion in *Pax2Cre/Ednrb* mutants. The one common feature of all hearing impaired *Pax2Cre/Ednrb* mutants was a reduction of SYP^+ vesicles, which is an indication of diminished synaptic activity. We observed diminished synaptic GluR2 in most but not all deaf mutants; this is a likely reason why vesicular transport was diminished in at least these mice. One possibility is that Ednrb regulates GluR2 expression or localization, although if so there are clearly additional mechanisms involved that account for normal GluR2 in hearing *Pax2Cre/Ednrb* mutants and as well in a small subset of deaf mutants.

We believe that genetic modifiers in the outbred ICR strain background of our colony account for the

variable penetrance of hearing impairment in global and conditional mutant backgrounds. Strain background can also explain variability in GluR2 localization in *Pax2Cre/Ednrb* mutants and perhaps also our observation of normal melanocyte presence in the stria vascularis compared to past reports. In most cases, a controlled inbred strain background is a benefit in terms of maintaining phenotypic consistency. However, as described here, the phenotypic uniformity of past studies is likely to have obscured other important features of auditory maturation that are under Ednrb control. We were able to recognize these new features in the outbred background of our colony by examining a very large number of mice for all phenotypes and by segregating them through lineage-specific conditional mutagenesis. It is obvious that *EDN3* and *EDNRB* mutations in humans have variable phenotypic presentation, which is a clear indication of the impact of modifier genes. Our colony resembles the human situation more accurately than any inbred background can replicate. New insights on the cell and molecular biology of auditory development that we are able to achieve with our colony may lead to new diagnostic criteria and perhaps also new therapeutic opportunities.

Materials and Methods

Animals. *Ednrb* (Rattner et al. 2013), *Edn3* (Baynash et al. 1994), *Wnt1Cre* (Danielian et al. 1998), *Pax2Cre* (Ohyama and Groves 2004), *Phox2bCre* (Scott et al. 2011) (JAX: 016223), *Tbx18Cre* (Cai et al. 2008), *Tie2Cre* (Kisanuki et al. 2001), *ROSA26*$^{CAG\text{-}tdTomato}$ (Madisen et al. 2010) (JAX: 007914), *ROSA26*$^{nT\text{-}nG}$ (Prigge et al. 2013) (JAX: 023537), *Ednrb-EGFP* (Gong et al. 2007) (MMRRC_010620-UCD) alleles have been described previously. All experiments with animals complied with National Institutes of Health guidelines and were reviewed and approved by the Medical University of South Carolina Institutional Animal Care and Use Committee. Wild-type ICR mice used for propagation of these lines were obtained

from Harlan/Envigo. All lines used in this study have been backcrossed for numerous generations to the ICR background, although because of intercrosses this was not rigorously controlled or quantified.

Auditory Brain Response (ABR) and Distortion Product of Otoacoustic Emissions (DPOAE). Postnatal day 19 mice were anesthetized with 3.0% isoflurane inhalation via a SomnoSuite small animal anesthesia system (Kent Scientific), and placed on a heating pad inside the SD1 small test enclosure (EST-LINDGREN). Needle electrodes were placed subcutaneously at the vertex (active), the ipsilateral ear (reference) and the pelvic limb (ground), and click-evoked ABR was recorded by the RZ6 signal processor (TDT) in declining 10dB steps beginning at 90dB. The ABR threshold was determined as the lowest intensity at which a representable ABR waveform could be identified. BioSigRZ Software (TDT) was used for ABR waveform (wave I amplitude and latency) analysis. DPOAE measurements were performed on selected ABR validated animals at P20. The acoustic probe containing the MF1 multi-field magnetic speakers (generating two continuous pure tones at the primary frequency f1 and f2; TDT) and the EB10^{+} DPOAE microphone (TDT) was placed in the ear canal, and DPOAE tests were performed on the range from 4kHz to 32kHz by the RZ6 signal processor (TDT). Acoustic responses and DPOAE amplitudes (f_{DP}=2f1-f2) with the noise floor (signal to noise ratio) were analyzed using BioSigRZ Software (TDT).

Cochlea preparation for histology and immunostaining. Postnatal day 20 mice were anesthetized and transcardially perfused with PBS followed by 4% paraformaldehyde. The inner ears were dissected, pierced at the apical wall of the cochlea, and postfixed in 4% PFA for 2 hr at room temperature. The entire inner ear was washed with PBS, decalcified in 8% EDTA (pH7.4) for 2-3 days, and then washed in

PBS. The whole tissue was embedded in 8% low melt agarose, then vibratome sectioned at 100μm thickness.

Immunofluorescence staining and imaging. Inner ear sections and wholemount cochlear preparations were cryoprotected with 30% sucrose/PBS, permeabilized by three freeze-thaw cycles, and washed extensively with PBS to remove sucrose. Tissues were incubated with primary antibodies at 37°C overnight, and then with Alexa Fluor secondary antibodies (Invitrogen) for 3-5 hours with gentle agitation. Primary antibodies used in this study include BLBP (1:500; Abcam ab32423), CtBP2 (1:500; BD 612044), GFP (1:3000; Abcam ab13970), GluR2 (1:300; Millipore MAB397), Hu (1:500; SCBT sc-28299), Kir4.1 (1:400; Alomone AGP-012), PECAM1/CD31 (1:200; BD 550274), Peripherin (1:200; Abcam ab99942), SYP (1:500, Abcam ab32594, 1:500, SCBT sc-17750), Tuj1 (1:1000; BioLegend MMS-435P). All immunostained sections/tissues were counterstained with DAPI, and then cleared in ScaleU2 (4M urea, 30% glycerol, 0.1% Triton-X 100). Fluorescence images were acquired using a Leica SPE confocal microscope system. To quantify IHC and OHC synaptic components, three images were acquired from base to middle turn of each cochlea and the number/volume of each fluorescence puncta was measured using the ImageJ Fiji plugin FociPicker3D. The average of three measurements per cochlea was used for compiling data. To quantify vesicular synaptophysin in SGNs, five confocal images (15μm apart) were extracted from z-stack images (1μm interval) from each tissue section, and SYP^+ area on each was measured by binary threshold selection using ImageJ normalized to the number of SGNs per image. The average of the five measurements per tissue was used for compiling data.

Statistics. All quantified data were graphed as mean±SEM, and analyzed for significance using a two-

tailed Student's t-test. Box and whisker plots show the mean, first and third quartiles. Any data point greater than third quartiles and less than first quartile were considered as outliers.

References

Barald KF, Kelley MW. 2004. From placode to polarization: new tunes in inner ear development. *Development* **131**: 4119-4130.

Baynash AG, Hosoda K, Giaid A, Richardson JA, Emoto N, Hammer RE, Yanagisawa M. 1994. Interaction of endothelin-3 with endothelin-B receptor is essential for development of epidermal melanocytes and enteric neurons. *Cell* **79**: 1277-1285.

Cai CL, Martin JC, Sun Y, Cui L, Wang L, Ouyang K, Yang L, Bu L, Liang X, Zhang X et al. 2008. A myocardial lineage derives from Tbx18 epicardial cells. *Nature* **454**: 104-108.

D'Amico-Martel A, Noden DM. 1983. Contributions of placodal and neural crest cells to avian cranial peripheral ganglia. *The American journal of anatomy* **166**: 445-468.

Dang R, Torigoe D, Suzuki S, Kikkawa Y, Moritoh K, Sasaki N, Agui T. 2011. Genetic background strongly modifies the severity of symptoms of Hirschsprung disease, but not hearing loss in rats carrying Ednrb(sl) mutations. *PloS one* **6**: e24086.

Danielian PS, Muccino D, Rowitch DH, Michael SK, McMahon AP. 1998. Modification of gene activity in mouse embryos in utero by a tamoxifen-inducible form of Cre recombinase. *Current biology : CB* **8**: 1323-1326.

Gettelfinger JD, Dahl JP. 2018. Syndromic Hearing Loss: A Brief Review of Common Presentations and Genetics. *Journal of pediatric genetics* **7**: 1-8.

Gong S, Doughty M, Harbaugh CR, Cummins A, Hatten ME, Heintz N, Gerfen CR. 2007. Targeting Cre recombinase to specific neuron populations with bacterial artificial chromosome constructs. *The Journal of neuroscience : the official journal of the Society for Neuroscience* **27**: 9817-9823.

Hanani M, Verkhratsky A. 2021. Satellite Glial Cells and Astrocytes, a Comparative Review. *Neurochemical research* **46**: 2525-2537.

Hosoda K, Hammer RE, Richardson JA, Baynash AG, Cheung JC, Giaid A, Yanagisawa M. 1994. Targeted and natural (piebald-lethal) mutations of endothelin-B receptor gene produce megacolon associated with spotted coat color in mice. *Cell* **79**: 1267-1276.

Huang S, Song J, He C, Cai X, Yuan K, Mei L, Feng Y. 2022. Genetic insights, disease mechanisms, and biological therapeutics for Waardenburg syndrome. *Gene therapy* **29**: 479-497.

Ida-Eto M, Ohgami N, Iida M, Yajima I, Kumasaka MY, Takaiwa K, Kimitsuki T, Sone M, Nakashima T, Tsuzuki T et al. 2011. Partial requirement of endothelin receptor B in spiral ganglion neurons for postnatal development of hearing. *The Journal of biological chemistry* **286**: 29621-29626.

Johnson SL, Safieddine S, Mustapha M, Marcotti W. 2019. Hair Cell Afferent Synapses: Function and Dysfunction. *Cold Spring Harbor perspectives in medicine* **9**.

Kisanuki YY, Hammer RE, Miyazaki J, Williams SC, Richardson JA, Yanagisawa M. 2001. Tie2-Cre transgenic mice: a new model for endothelial cell-lineage analysis in vivo. *Developmental biology* **230**: 230-242.

Ladher RK, O'Neill P, Begbie J. 2010. From shared lineage to distinct functions: the development of the inner ear and epibranchial placodes. *Development* **137**: 1777-1785.

Madisen L, Zwingman TA, Sunkin SM, Oh SW, Zariwala HA, Gu H, Ng LL, Palmiter RD, Hawrylycz MJ, Jones AR et al. 2010. A robust and high-throughput Cre reporting and characterization system for the whole mouse brain. *Nature neuroscience* **13**: 133-140.

Matsushima Y, Shinkai Y, Kobayashi Y, Sakamoto M, Kunieda T, Tachibana M. 2002. A mouse model of Waardenburg syndrome type 4 with a new spontaneous mutation of the endothelin-B receptor gene. *Mammalian genome : official journal of the International Mammalian Genome Society* **13**: 30-35.

Mueller JL, Goldstein AM. 2022. The science of Hirschsprung disease: What we know and where we are headed. *Seminars in pediatric surgery* **31**: 151157.

Ohyama T, Groves AK. 2004. Generation of Pax2-Cre mice by modification of a Pax2 bacterial artificial chromosome. *Genesis* **38**: 195-199.

Pingault V, Ente D, Dastot-Le Moal F, Goossens M, Marlin S, Bondurand N. 2010. Review and update of mutations causing Waardenburg syndrome. *Human mutation* **31**: 391-406.

Prigge JR, Wiley JA, Talago EA, Young EM, Johns LL, Kundert JA, Sonsteng KM, Halford WP, Capecchi MR, Schmidt EE. 2013. Nuclear double-fluorescent reporter for in vivo and ex vivo analyses of biological transitions in mouse nuclei. *Mammalian genome : official journal of the International Mammalian Genome Society*.

Rattner A, Yu H, Williams J, Smallwood PM, Nathans J. 2013. Endothelin-2 signaling in the neural retina promotes the endothelial tip cell state and inhibits angiogenesis. *Proceedings of the National Academy of Sciences of the United States of America* **110**: E3830-3839.

Read AP, Newton VE. 1997. Waardenburg syndrome. *Journal of medical genetics* **34**: 656-665.

Reijntjes DOJ, Pyott SJ. 2016. The afferent signaling complex: Regulation of type I spiral ganglion neuron responses in the auditory periphery. *Hearing research* **336**: 1-16.

Scott MM, Williams KW, Rossi J, Lee CE, Elmquist JK. 2011. Leptin receptor expression in hindbrain Glp-1 neurons regulates food intake and energy balance in mice. *The Journal of clinical investigation* **121**: 2413-2421.

Steel KP, Barkway C. 1989. Another role for melanocytes: their importance for normal stria vascularis development in the mammalian inner ear. *Development* **107**: 453-463.

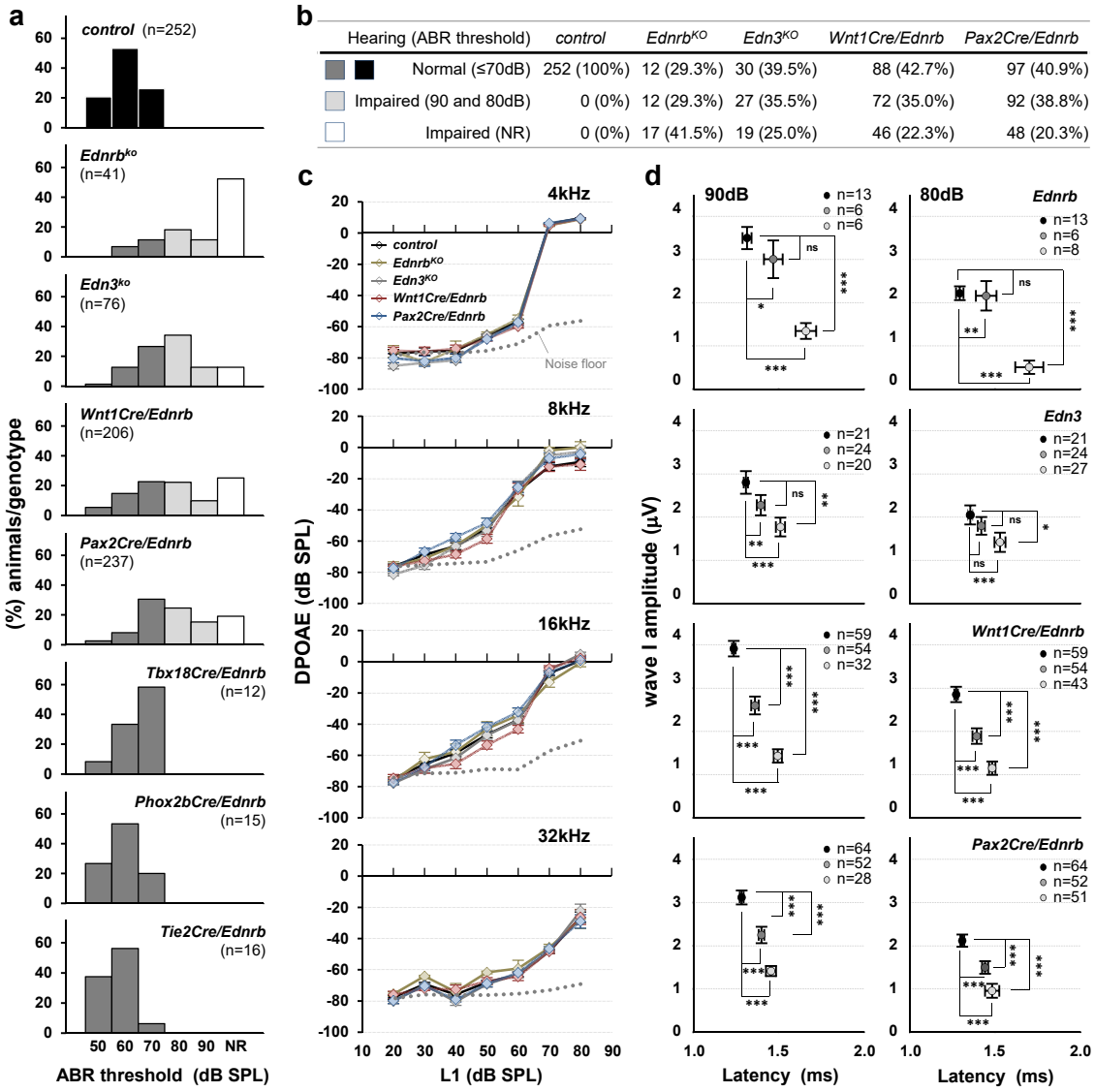

Hearing (ABR threshold)	control	Ednrb^KO	Edn3^KO	Wnt1Cre/Ednrb	Pax2Cre/Ednrb
Normal (≤70dB)	252 (100%)	12 (29.3%)	30 (39.5%)	88 (42.7%)	97 (40.9%)
Impaired (90 and 80dB)	0 (0%)	12 (29.3%)	27 (35.5%)	72 (35.0%)	92 (38.8%)
Impaired (NR)	0 (0%)	17 (41.5%)	19 (25.0%)	46 (22.3%)	48 (20.3%)

Figure 1. Incomplete penetrance of hearing impairment in Edn3-Ednrb signaling deficient mice. (a) Compiled representation of the percentage of mice of each genotype that exhibited the indicated ABR threshold. Black bars, genetic controls (see also Supplemental Table S1); dark grey bars, hearing mutants; light grey bars, hearing impaired mutants (ABR threshold 80-90dB); white bars, non-hearing mutants (NR=no response at the highest stimulus intensity (90dB)). (b) Table summarizing number of animals tested and phenotype frequency for global *Ednrb*, global *Edn3*, *Wnt1Cre/Ednrb* and *Pax2Cre/Ednrb* mutant mice. (c) Mean DPOAE (±SEM) at the indicated frequency (kHz) in controls (n=26) and selected hearing impaired (ABR threshold≥80dB) *Ednrb* (n=8), *Edn3* (n=15), *Wnt1Cre/Ednrb* (n=15) and *Pax2Cre/Ednrb* (n=13) mutants. (d) Mean amplitude vs latency plots for wave I in ABR waveforms at 90dB (left) and 80dB (right) acquired from selected hearing mutants (ABR threshold≤70dB, dark grey); hearing impaired mutants (left, ABR threshold 80-90dB, light grey; right, ABR threshold=80dB, light grey) and their littermate controls (black). Error bars; ±SEM. p-values; *$p<0.05$, **$p<0.01$, ***$p<0.001$, ns=not significant.

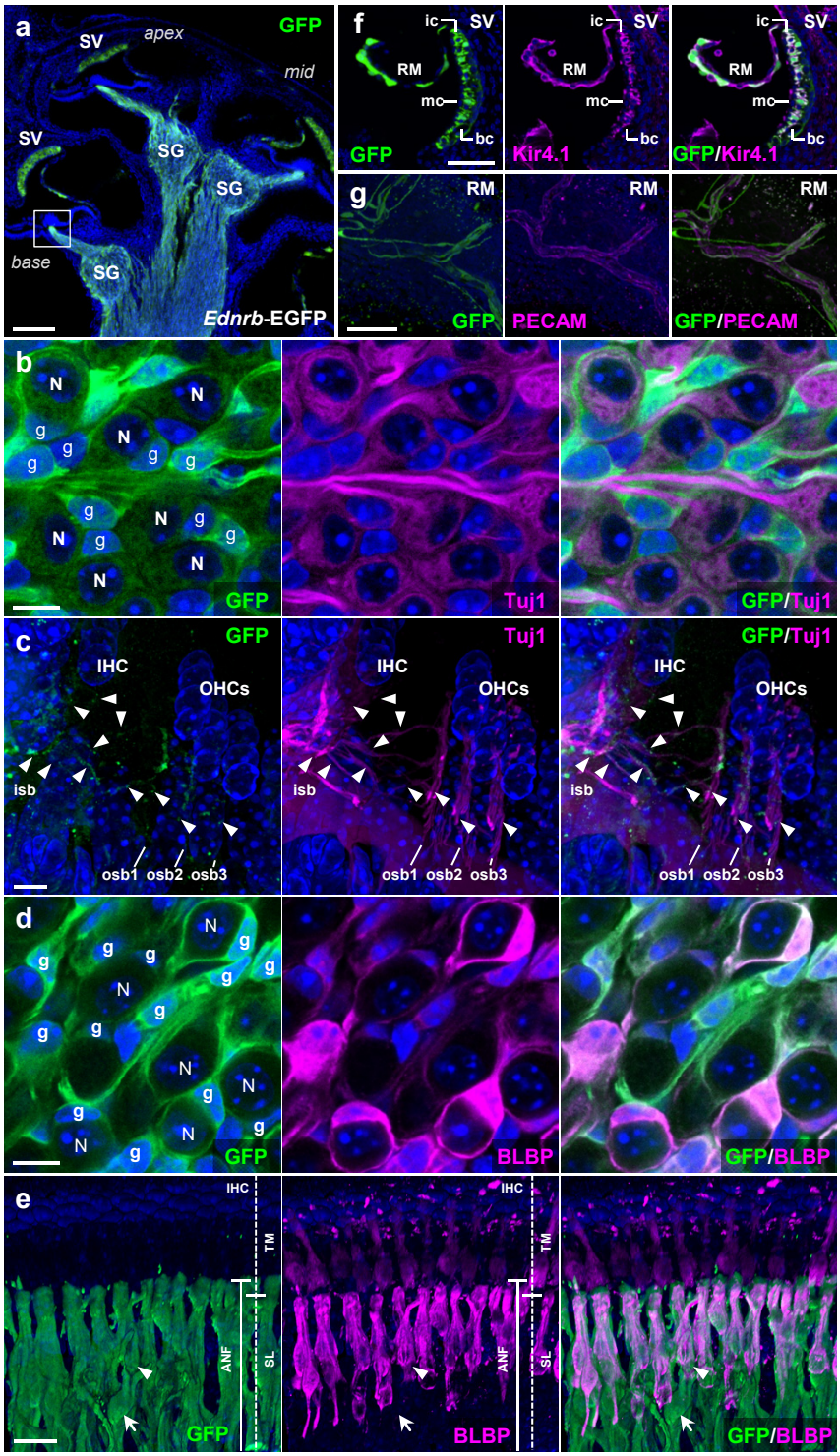

Figure 2. Ednrb expression in P7 cochlea. Sagittal sections of cochlea isolated from P7 Ednrb-EGFP BAC transgenic mice stained for GFP only (green; a) or co-stained for neuronal Tuj1 (magenta; b-c), glial BLBP (magenta; d), inward rectifier potassium channel Kir4.1 (magenta; e), and vascular endothelial PECAM (magenta; f). High magnification views demonstrate Ednrb expression in SGN cell bodies (b) and peripheral axons (c), in glia (d), in Kir4.1^{+} intermediate and Kir4.1^{-} basal stria cells (f), and in vascular endothelial cells of the Reissner's membrane (g). Arrowheads in (c) denote GFP^{+} axons that innervate the inner and outer hair cells. "N" and "g" in (b) and (d) denote spiral ganglion neurons and glia, respectively. GFP signal is stronger in glia than in neurons. (e) Whole-mount preparation of P7 Ednrb-EGFP stained for GFP (green) and BLBP (magenta) visualizing magnified view of BLBP^{+} Schwann cells corresponding to the boxed area in (a). Abbreviations: ANF, auditory nerve fibers; bc, basal cell; ic, intermediate cell; IHC, inner hair cell; isb, inner spiral bundle; mc, marginal cell; OHC, outer hair cell; osb, outer spiral bundle; RM, Reissner's membrane; SG, spiral ganglion; SV, stria vascularis. Scale bars: 200mm (a), 10μm (b-d), 25μm (e), 100μm (f), 50μm (g).

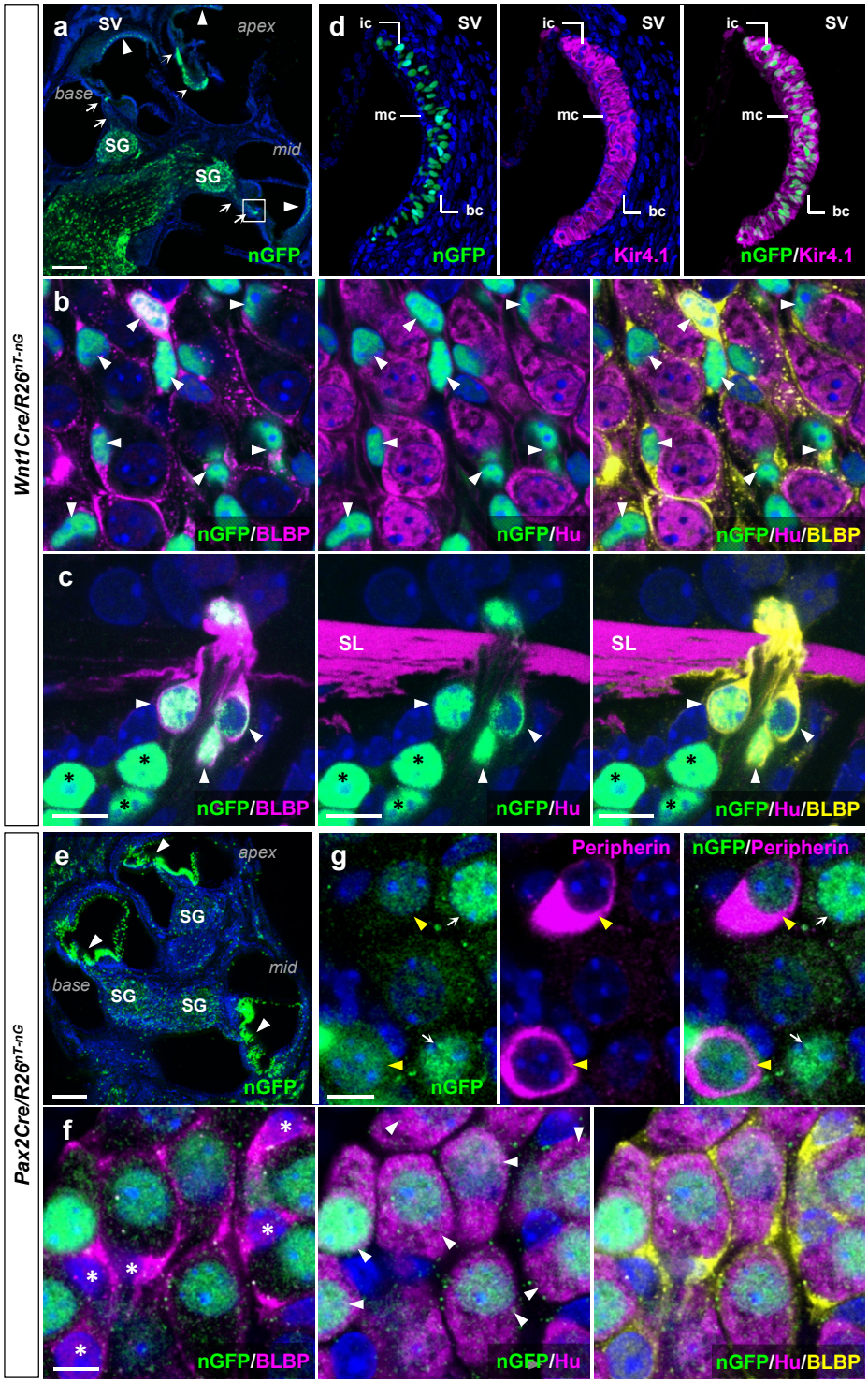

Figure 3. *Wnt1Cre* and *Pax2Cre* delineate distinct cell types in the cochlea. Sagittal sections of cochlea isolated from P7 *Wnt1Cre/R26*$^{nT\text{-}nG}$ (a-d) and *Pax2Cre/R26*$^{nT\text{-}nG}$ (e-g) mice stained for GFP (a) and costained for neuronal Hu (b-c, f), glial BLBP (b-c, f), Kir4.1 (d), and type II neuron specific Peripherin (g). (a) Reporter recombination (nuclear GFP) driven by *Wnt1Cre* occurs in the stria vascularis (arrowheads), and in the spiral ganglion and along their nerve trajectories (arrows). (b) High magnification view of spiral ganglia in (a) shows *Wnt1Cre* is active in BLBP^{+} satellite cells (arrowheads) but not in Hu^{+} SGNs. (c) A magnified view of the boxed area in (a). *Wnt1Cre* labels BLBP^{+} (arrowheads) and BLBP^{-} (black asterisks) Schwann cells (Hu^{-}) along the auditory fibers. (d) A magnified view of the stria vascularis in (a) shows the activity of *Wnt1Cre* in Kir4.1^{+} intermediate stria cells. (e) Reporter recombination by *Pax2Cre* occurs in vast majority of cochlear epithelium (arrowheads) and in the spiral ganglion. (f-g) High magnification views of spiral ganglia in (e) demonstrate that *Pax2Cre* is exclusively active in Hu^{+} SGNs (f; white arrows) including Peripherin^{+} type II neurons (g; yellow arrows) but not in BLBP^{+} satellite cells (f; asterisks). Abbreviation; SL, spiral lamina. Scale bars; 200μm (a, d),10μm (b, e-f), 100μm (c).

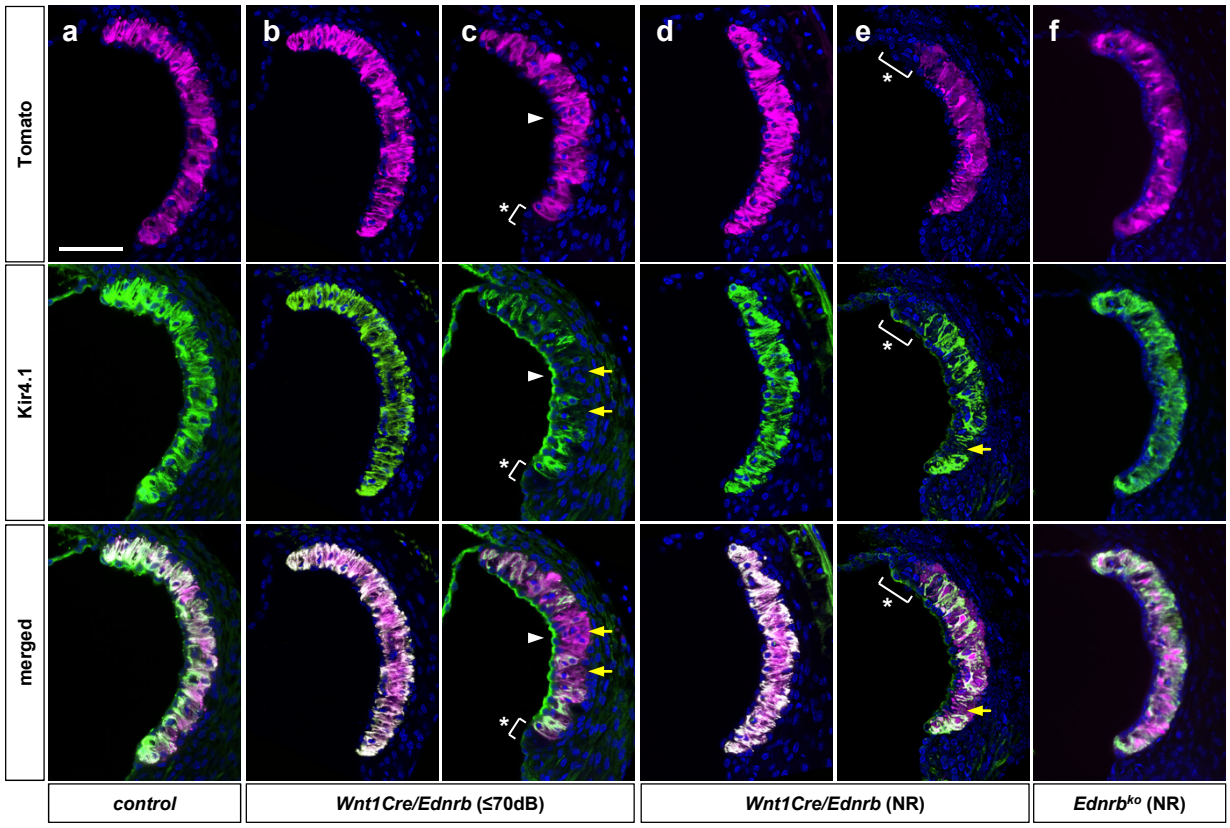

g

Wnt1Cre⁺ cell contribution and maturation	*control*	*Wnt1Cre/Ednrb* (≤70dB)	*Wnt1Cre/Ednrb* (≥90dB)	*Ednrb*^{ko} (≥90dB)
% normal	100 (12/12)	83.3 (5/6)	80.0 (12/15)	100 (2/2)
% partial loss	0 (0/12)	16.7 (1/6)	20.0 (3/15)	0 (0/2)
% total loss	0 (0/12)	0 (0/6)	0 (0/15)	0 (0/0)

Figure 4. Contribution of *Wnt1Cre*-labeled melanocytes to the Kir4.1⁺ intermediate stria cells in hearing and hearing impaired *Ednrb*-deficient mice. Confocal (z-stack) images of the stria vascularis of P19 hearing (ABR threshold≤70dB) *Wnt1Cre/Ednrb/R26*$^{td\text{-}Tomato}$ mutant (b-c), hearing impaired (ABR threshold=NR) *Wnt1Cre/Ednrb/R26*$^{td\text{-}Tomato}$ mutants (d-e), a littermate control (a), and hearing impaired (ABR threshold=NR) global *Ednrb* mutant crossed into the *Wnt1Cre/R26*$^{td\text{-}Tomato}$ background (f). (c, e) Asterisks denote the portion of the stria vascularis that does not contain *Wnt1Cre* lineage derived Kir4.1⁺ intermediate cells. Arrows point out *Wnt1Cre* lineage⁺ cells that are lacking Kir4.1 expression. Arrowheads point out missexpression or misslocalization of Kir4.1 at the apical surface of the marginal stria cells. Scale bar: 100μm. (g) Table summarizing the number of animals tested and the phenotype (intermediate cell number and maturation) frequency for *Wnt1Cre/Ednrb* and global *Ednrb* mutant mice.

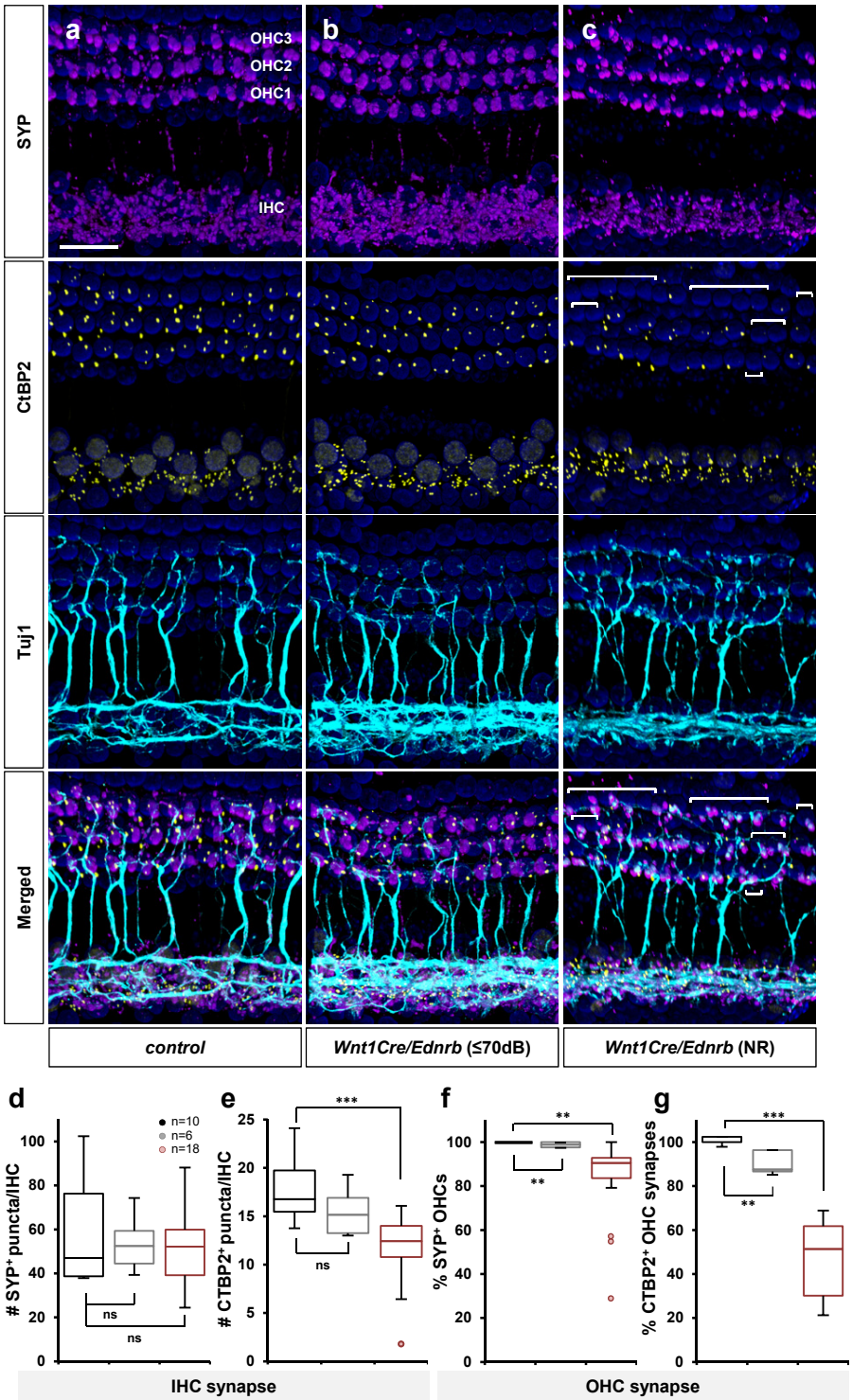

Figure 5. Defective ribbon synapse formation in hearing impaired *Wnt1Cre/Ednrb* mutant mice. Whole-mount preparations of cochlea isolated from P19 *Wnt1Cre/Ednrb* mutant mice (b-c) and a littermate control (a) immunostained for postsynaptic SYP (magenta), presynaptic CtBP2 (yellow), and neuronal Tuj1 (cyan). The image shown in (c) is from a hearing impaired *Wnt1Cre/Ednrb* mutant of median synaptic phenotype. Yellow arrows denote the absence of SYP staining at the OHCs. OHCs in the bracketed areas lack CtBP2$^+$ synaptic ribbons. Scale bar: 10µm. (d-e) Box and whisker plots for the number of SYP$^+$ (d) and CtBP2$^+$ (e) puncta per IHC in control (black), hearing *Wnt1Cre/Ednrb* mutant (grey), and hearing impaired *Wnt1Cre/Ednrb* mutant (ABR threshold ≥80dB; red) mice. (f-g) Box and whisker plots for the percentage of OHCs with postsynaptic SYP$^+$ staining (f) and presynaptic CtBP2$^+$ staining (g) in control (black), hearing *Wnt1Cre/Ednrb* mutant (grey), and hearing impaired *Wnt1Cre/Ednrb* mutant (ABR threshold ≥80dB; red) mice. p-values: $^{**}p<0.01$, $^{***}p<0.001$, ns=not significant.

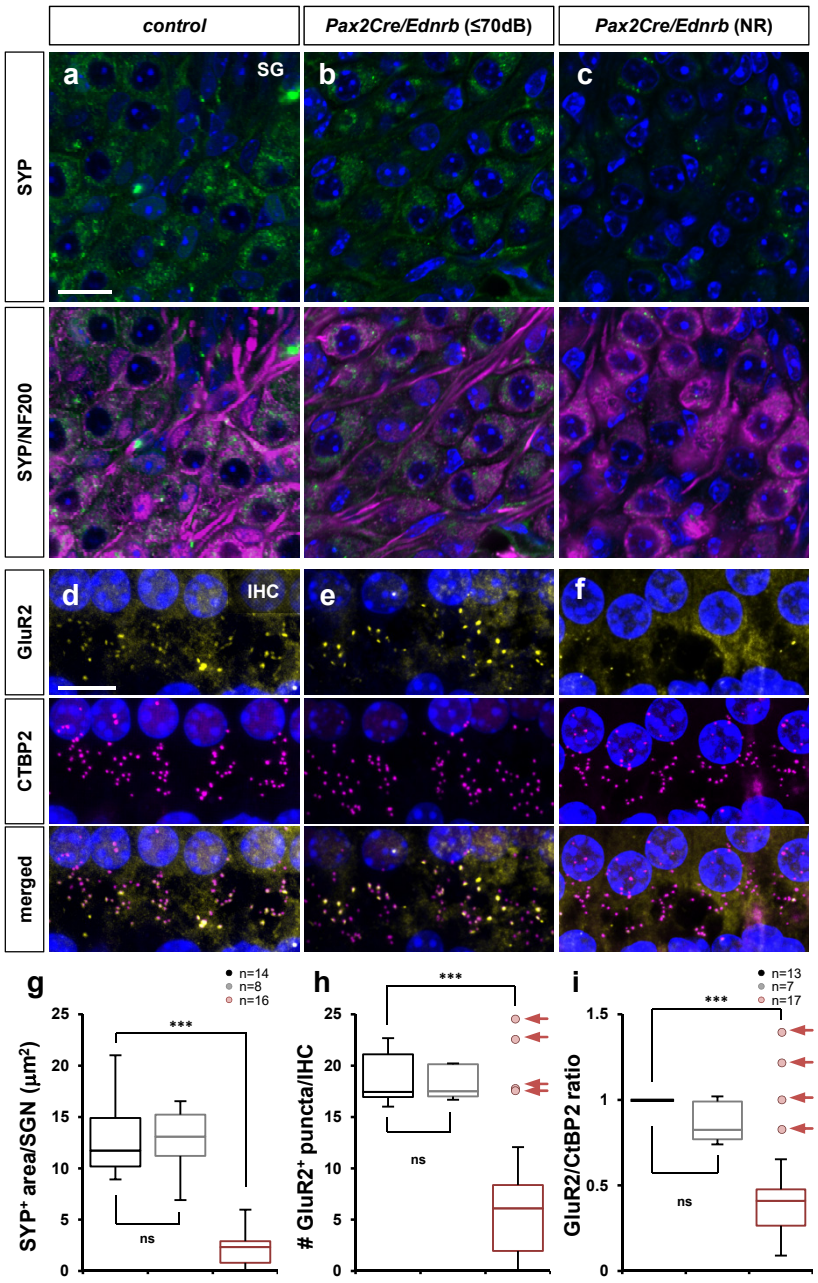

Figure 6. Defective SGN activation in hearing impaired *Pax2Cre/Ednrb* mutant mice. (a-c) High magnification views of P19 spiral ganglion sections from hearing *Pax2Cre/Ednrb* (b), hearing impaired *Pax2Cre/Ednrb* (c) mutant mice and a littermate control (a) immunostained for SYP (green), and NF200 (magenta). Compiled representation of SYP$^+$ area per SGN in each group is shown in g. (d-f) Whole-mount preparation of cochlea isolated from P19 hearing *Pax2Cre/Ednrb* (e), hearing impaired *Pax2Cre/Ednrb* (f) mutants and a littermate control (d) immunostained for GluR2 (yellow), and CtBP2 (magenta). Compiled representation of GluR2$^+$ puncta number per IHC and GluR2/CtBP2 ratio per IHC are shown in h and i, respectively. Scale bars: 10µm. (g) Box and whisker plots for the SYP$^+$ area per SGN in control (black), hearing *Pax2Cre/Ednrb* mutant (grey) and hearing impaired mutant (ABR threshold=NR; red) mice. (h-i) Box and whisker plots for the number of GluR2$^+$ puncta per IHC (h) and GluR2/CtBP2 ratio (i) in control (black), hearing *Pax2Cre/Ednrb* mutant (grey) and hearing impaired mutant (ABR threshold=NR; red) mice. Arrows in (h) and (i) represent hearing impaired *Pax2Cre/Ednrb* mutants exhibiting a normal GluR2 profile at the IHC synapse. p-values: $^{**}p<0.01$, $^{***}p<0.001$, ns=not significant.